Ground state of solid hydrogen at high pressures

D. M. Ceperley and B. J. Alder
Lawrence Livermore National Laboratory, University of California, Livermore, California 94550
(Received 13 March 1987)

Quantum Monte Carlo calculations of the properties of bulk hydrogen at zero temperature have been performed. The only approximations involved in these calculations are the restriction to finite systems (64 to 432 atoms), the use of the fixed-node approximation to treat Fermi statistics, and the finite length of the Monte Carlo runs. The Born-Oppenheimer approximation was avoided by solving the quantum many-body problem simultaneously both for the electron and proton degrees of freedom. Using different trial functions and several different crystal structures the transition between the explored molecular and atomic phases was determined to occur at 3.0 ± 0.4 Mbar. The transition to a rotationally ordered molecular phase occurred at about 1.0 Mbar. A lower bound to the static dielectric constant, given in terms of the static structure factor, was found to lie close to experimental values and became large for pressures greater than 500 kbar.

I. INTRODUCTION

The properties of bulk hydrogen have yet to be calculated from first principles, even though it is the simplest of the elements. There is a long tradition of calculations of the structure and properties of hydrogen dating back at least to the pioneering work of Wigner and Huntington[1] in 1935. They predicted that hydrogen will undergo a molecular to atomic transition as the density is increased and estimated that this transition occurs above a pressure of 0.25 Mbar. While the sophistication and accuracy of the calculations of the atomic phase have increased over the years, the knowledge of the equation of state of the molecular phase still comes primarily from experiment. Recent diamond-anvil measurements[2,3] have increased this knowledge to pressures close to 1 Mbar, and there are good prospects for experiments to still higher pressures. In addition, shock-wave experiments[4] have determined some properties of hydrogen at Mbar pressures, but at much higher temperatures (10^4 K). To date, there has been no reproducible observation of the transition of hydrogen into the atomic phase. One of the goals of this paper is to calculate from first principles this transition density and pressure.

For pressure of less than 100 kbar, the molecules of hydrogen in the molecular crystal are relatively undistorted from their state in the vacuum.[5] Consequently, up to these pressures the angular momentum of a single molecule is almost a good quantum number and the molecules are almost freely rotating at zero temperature so that the rotation of nearby molecules are mutually independent. However, at higher pressures it becomes energetically favorable for the molecular axes to align relative to each other. This transition has been observed[6] to occur in deuterium at a pressure of 280 kbar but it has not yet been observed in hydrogen. Because this transition involves a small energy change, it is possible to calculate the transition density only crudely.

Other possible transitions in hydrogen at zero temperature have been proposed. It is possible, through a mechanism known as band crossing, for molecular hydrogen to become metallic before the transition to an atomic metal. Such a transition occurs in iodine. Calculations based on density-functional theory have predicted[7] that such band crossing will occur in hydrogen at 9-fold compression ($r_s = 1.48$). In these calculations, the distortions of the molecules due to pressure have not been included, so their reliability is unclear. Although the present method avoids these approximations, the investigation of this particular transition is postponed to a future publication.

Another transition that has been proposed[8] is that of melting of the atomic solid to an atomic liquid. Such a transition is inevitable at enormously high pressures, but it has been argued that it could occur at relatively low pressures due to electron screening of the proton-proton interaction. In support of this mechanism, band-structure calculations[9] of metallic hydrogen at relatively low densities (which, however, neglect the zero-point motion of the protons) find a highly distorted, low-symmetry lattice as giving the minimum-energy structure. However, these distorted lattices have higher energy when the proton zero-point energy is added.

To resolve these questions an accurate computational method is required, that can determine the properties and energy of hydrogen in these various phases. The quantum Monte Carlo method is such a promising technique and has been successfully employed to determine the properties of such diverse systems as liquid and solid helium,[10] small chemical molecules,[11] and the electron gas,[12] including the melting of the latter. The simulation by Monte Carlo calculations of hydrogen is a natural extension of these studies. In fact, hydrogen is simulated simply as a two-component system of charged particles with unequal masses. Such a simulation in the experimentally accessible regime allows an unambiguous comparison of experiment with theory, perhaps for the first time on a many-body system. Previous comparisons of such simulation results with experiments have involved empirically determined interatomic potentials or other simplified Hamiltonians.

One advantage of the Monte Carlo method is that the zero-point motion of the protons can be treated exactly in

both the molecular and atomic phases. Another is that the accuracy of the results can be determined by statistical means within the calculation itself. To make the error bars small requires a great deal of computer time. However, the human time needed to set up the calculation is probably less than for the other types of methods; particularly since the same program works for all phases and, in principle, for any combination of elements. In practice, the method as so far developed is only practical for low-Z elements. These simulations became only practical when computers of the speed of the Cray Research Cray-I computer were available. The amount of computer time needed (a few hours of central-processing unit time for each density) will not be as large in the near future, particularly as cheap and fast parallel processors become widespread. It will be possible to do much more refined calculations than presented here as computers and the methodology improve.

The main difficulties and limitations of the quantum Monte Carlo method are its restriction to a small number of atoms (less than a few hundred), the difficulty of determining the most stable crystal structure at a fixed density, the slow motion of the protons relative to the electrons, the upper-bound aspect of the fixed-node approximation, and the transient nature of the release-node method for fermions.

In Sec. II the Monte Carlo methods used in this paper will be briefly discussed. Section III presents the crucial choice of the trial function used in the various phases of hydrogen. Section IV contains the results of the simulations in the molecular phase, Sec. V in the metallic phase, Sec. VI introduces the conductivity, and Sec. VII presents a summary.

Throughout this paper energies are in units of Rydbergs/hydrogen atom and densities are in r_s units, where $4\pi a^3/3=v$ and $r_s=a/a_0$, where a_0 is the Bohr radius and v is the volume of an hydrogen atom, that is $r_s^3=1.338v_m$, where v_m is in units of cm^3/mole H_2.

II. NUMERICAL METHOD

Since the quantum Monte Carlo methods used here have been already discussed in detail elsewhere, we will simply define the three types of methods used on this problem, namely the following.

(i) *Variational Monte Carlo (VMC):* Let $\Psi(R)$ be a known trial function, where R refers to the full $3N$ set of particle coordinates and N is the total number of particles. Then VMC uses the Metropolis algorithm[13–15] to sample $|\Psi|^2$ and thus any expectation value with respect to this trial function can be computed, the most important of which is the variational energy of the trial function. The VMC method is used to select a good trial function, by minimizing the variational energy with respect to parameters in the trial function, and to initialize the ensemble for methods (ii) and (iii). VMC has the advantage in that it is considerably faster than the other two methods, a factor of 10 is typical, and there are no difficulties with fermions. However, it only yields an upper bound, not the true ground-state energy.

(ii) *Fixed-node diffusion Monte Carlo (DMC).* The Schrödinger equation in imaginary time, and transformed by the trial function is

$$\frac{\partial f(R,t)}{\partial t}=\sum_{j=1}^{N}\frac{\hbar^2}{2m_j}\nabla_j(\nabla_j f-f\nabla_j \ln\Psi^2) -(\Psi^{-1}H\Psi-E_T)f\ , \tag{1}$$

where E_T is the trial energy. The DMC algorithm[11,12] interprets $f(R,t)=\Psi(R)\phi(R,t)$ as a probability distribution in configuration space. The function $\phi(R,t)$ tends at large "time" t to the ground-state wave function. An initial ensemble of several hundred points with density $f(R,0)=\Psi(R)^2$, is evolved forward in "time." The three terms on the right-hand side then correspond to diffusion (with a diffusion constant equal to $\hbar^2/2m_j$), a drift derived from the trial function, and branching. For fermions, to interpret f as a probability, one also assumes that the nodes of the ground-state wave function are identical to the nodes of the trial function, so that their product, f, is always positive. This converts the fermion system to a distinguishable particle system. With this restriction, it can be shown[16] that the calculated energy is an upper bound to the exact ground-state energy.

In DMC, an additional approximation is made in "solving" Eq. (1). It is assumed that the drift and the local energy are constant in the region about the current position. This is only valid if the time step is small enough, so in practice, simulations for several different time steps need to be performed to test the accuracy of the simulations. More details of this algorithm are given in Ref. 11.

After convergence in time is reached, that is t is large enough so that the steady-state solution of Eq. (1) is obtained, the probability distribution of points in the ensemble is $\phi(R)\Psi(R)$. This is called the *mixed distribution* since it contains information about both the exact ground state, $\phi(R)$ (with the fixed-node restriction) and the trial function. The ground-state energy is the average value of $H\Psi/\Psi$, averaged over this mixed distribution, and has the *zero variance property* of quantum Monte Carlo; since as $\Psi(R)$ approaches an exact eigenfunction, the variance of the MC estimate of the energy approaches zero. Thus, energies in QMC can be calculated more accurately than for classical systems since the accuracy depends only on the accuracy of the trial function.

If the radial distribution function, $g(r)$, or any other average over the wave function other than the total energy is calculated using the mixed distribution, the result is somewhere between the variational $g(r)$ and the exact $g(r)$. In fact, if the trial function is sufficiently accurate the mixed pair correlation function should be halfway in between. Linear extrapolation[17] is the simplest way of calculating averaged quantities other than the energy, that is:

$$g(r)=2g_{\rm mix}(r)-g_{\rm var}(r)\ . \tag{2}$$

(iii) *Green's-function Monte Carlo (GFMC).* This combined with the release-node method for treating Fermi statistics is an exact procedure; that is it completely removes the two approximations discussed above.[17,18] The method is practically only convergent, however, for sys-

tems where the Fermi energy is sufficiently close to the Bose energy and the trial function has reasonably accurate nodes. Both of these assumptions are satisfied for hydrogen up to quite high densities (a few Mbar) as checked here by Monte Carlo calculations. Because the GFMC method is the slowest of the three methods, it was not possible to use it for all of the calculations, but only to benchmark the DMC runs.

There are additional complications to be considered in these calculations which will be mentioned here and discussed later. First, the results for finite systems must be extrapolated to the bulk limit. To minimize the finite-size effects, the calculations are always performed using periodic boundary conditions. Because the Coulomb interaction as well as the many particle correlations in the trial function are long ranged, the Ewald image potential summation[19] must be used. Nevertheless, whenever the electrons are delocalized, there still remains an appreciable dependence of the properties on the size of the system, which can be traced to the discontinuity in the momentum distribution at the Fermi surface. This dependence is removed by an extrapolation based on Fermi-liquid theory.

Secondly, because the proton is 1836 times more massive than the electron, its diffusion with the DMC or GFMC algorithm (but not VMC) is that much slower, and its root-mean-square displacement per step is hence 42 times smaller than that of the electron. While the electronic distribution converges rapidly to its ground state, it is easy to find situations where the protonic distribution does not equilibrate in a reasonable amount of computer time. In principle, the simulations for the electron-proton system should be thousands of times longer than for a one-component system, and that is not practical. It is only possible with present computers to make one order of magnitude longer runs than that for the electrons alone. Several things can be done to improve the rate of convergence and establish a test for it, short of finding a general procedure to remove the disparate time scale problem. The initial ensemble should be thoroughly equilibrated by VMC so that for accurate trial functions the proton distribution will, in fact, be close to its final equilibrium value. In crystal phases the motion of the protons is severely limited in any case, so that the relevant time for equilibration is much shorter, namely the inverse of the Debye temperature. Some care has been taken to make the proton trial function accurate. For example, at low density an accurate approximation to the exact proton-proton molecular wave function has been used. To test for convergence, very long runs have been made on small systems of eight atoms.

Convergence to the state of lowest energy is also inhibited by the initial conditions, that is, for example, by the assumed crystal structure and by the nature of the trial function. Both of these conspire to keep the points of the random walk in the region of phase space appropriate to the initially selected phase. Although a constant pressure ensemble[20] instead of the constant volume ensemble used here could, in principle, partially overcome this difficulty, it is not yet clear whether that method can in reasonable computer time make the transition to the most favorable phase. For the constant volume ensemble each crystal structure must be tested separately. The ground state at a given density is then the one with the lowest energy. By this procedure it is certainly possible that a relevant phase, particularly of crystalline molecular hydrogen at high pressure, has been missed. Furthermore, phase transitions often involve very small energy differences. Since even with long runs the error bars on our calculations are roughly 0.001 Ry/atom, phase transitions driven by energies less than this are not capable of being resolved by this direct quantum Monte Carlo method. The development of differential Monte Carlo could circumvent this difficulty.

III. THE TRIAL FUNCTION

A trial function is selected to be as good an approximation as possible to the ground state, however, the function must be quick to evaluate on the computer as well, since at each step of the random walk the trial function and its first and second derivatives must be evaluated. Since the protons are not in a periodic array because of their zero-point motion, conventional band functions are not appropriate. Pair-product or Slater-Jastrow trial functions are employed because they have been found to be quite accurate in studies of the electron gas,[19] helium[10], and chemical molecules.[11]

$$\Psi(R)=\exp\left[\sum_{i<j}u_{ij}(r_{ij})\right]\prod_{\sigma}D_{\sigma}\ , \tag{3}$$

where $u_{ij}(r)$ is the "pseudopotential" acting between particles i and j a distance r apart and D_σ is the Slater determinant of a group of particles σ. Therefore,

$$D_\sigma=\det\{\phi_k(r_j)\} \tag{4}$$

and $\phi_k(r)$ is the kth orbital function. In principle, there should be four determinants in Eq. (3); two for electrons and two for protons, each with up or down spin. However, for the phase of hydrogen considered in this paper, the protons are always localized and hence distinguishable to a high degree of accuracy, so their antisymmetric exchange can be ignored.

The trial function of Eq. (3) contains three pseudopotentials, that acting between two electrons, between two protons, and between an electron and a proton. In addition, there are orbitals for both the electrons and for the protons. It is impractical to parametrize these functions and then find by brute force the optimal such trial function, as the dimensionality of the search for all the parameters of the pseudopotentials and orbitals is too high. For simpler problems, such as the electron gas and liquid helium, the optimal pseudopotential has been determined within the hypernetted chain approximation.[21] However, the simple integral equations are not sufficiently accurate for hydrogen and they would be much more complicated to solve numerically for a mixture of electrons and protons in a crystalline phase.

For the electron gas it was found[19] that pseudopotentials derived from the random-phase approximation (RPA) gave quite reasonable trial functions, and these RPA pseudopotentials are also found to be acceptable for

hydrogen, as will be demonstrated. The RPA pseudopotentials[22] are derived from an expression for the variational energy in momentum space in which all terms involving three wave vectors are dropped (the RPA approximation). The structure function is related to the Hartree-Fock structure function by perturbation theory and then the energy is minimized with respect to the pseudopotentials. These RPA functions have the exact limiting behavior both when any two particles approach each other, the cusp condition, and when they are far apart. The RPA functions contain no adjustable parameters. A derivation will be published elsewhere.

The electron and proton orbitals that go into the Slater determinants define the phase of the system. Electron orbitals in crystals can either be described as delocalized band functions or by Wannier functions and these two descriptions are equivalent. However, there may be significant numerical advantages to one description or the other. In the atomic crystal the electrons are delocalized with a nearly spherical Fermi surface. Under these circumstances the s-wave scattering of the electrons by the protons can be accounted for by a pseudopotential so that the orbitals will be very close to that of the homogeneous electron gas, namely plane waves. The equivalent Wannier functions are less appropriate since these functions decay slowly in real space, as r^{-3}, and are difficult to construct for finite systems because of boundary effects. On the other hand, in the molecular phase, Wannier functions are a much more compact representation of the wave function but a plane-wave expansion of a molecular wave function would involve many plane waves. It has been shown[23] in one-electron theory that Wannier functions for systems with band gaps are exponentially localized. However, an even simpler compact form has been found[11] to describe the electronic hydrogen wave function well, namely a single Gaussian centered at the middle of the bond. Gaussians were hence used for the molecular phase.

$$\phi_k(r)=\exp[-C_e(r-Z_k)^2]\ , \tag{5}$$

where the lattice sites, Z_k, were chosen appropriate to several crystal structures. These orbitals are not orthogonal, orthogonality is not essential with the Monte Carlo approach. The variational parameter C_e was chosen by minimizing the energy in a variational calculation.

For the proton orbitals, Gaussians were also used with one proton per lattice site in the atomic phase and two protons per lattice site in the molecular phase. The protons were treated as distinguishable particles, so the assignment to lattice sites was fixed at the beginning of the calculation. The electrons are of course free to exchange between different molecules. As for the pseudopotential between protons it was found in the molecular phase that the RPA approximation between protons within the same molecule did not work very well. The correlation energy represented by the proton-proton pseudopotential is quite small (about 0.01 Ry) but it is highly desirable to start with a quite accurate proton trial function so that the random walk will converge quickly. A better approximation is the Born-Oppenheimer wave function for an isolated hydrogen molecule, the proton-proton part of which can be well approximated by

$$\phi(r)=\exp\{-[b_1/(b_2+r)]^{b_3}-b_4r\}/r \tag{6}$$

with the values of the parameters b_1, b_2, b_3, and b_4 equal, respectively, to 8.046, 3.0, 4.456, and 14.56 and the units of r and the b's are in bohr radii. The first term in the exponent corresponds to the repulsion of the protons and the second to the covalent binding. This simple function gives about 95% of the proton correlation energy in an isolated molecule. The variational energy of an isolated molecule, using Eq. (6) for the proton orbital and Eq. (5) for the electron orbital, is -1.157 a.u.; the exact value is -1.164 a.u.

When a molecule is incorporated into a solid, some changes have to be made. First of all, a repulsion acts between protons of different molecules. The first term in the exponent of Eq. (6) is used for that. Furthermore, since two protons are bound, via Eq. (5), onto one lattice site, a term is added to the pseudopotential to cancel out this extra proton-proton binding. This is achieved by writing the wave function for the two protons in a molecule in relative and center-of-mass coordinates. The pseudopotential depends only on the relative coordinates, while fixing of the molecule to the lattice site only depends on center of mass coordinates. Finally, a term is added to the trial function which orients the molecule in a crystal direction. The simplest function with the appropriate symmetry is $\cos^2(\theta)$, where θ is the angle between the molecular axis and a crystal direction. For the fcc lattice these crystal axes are body diagonals $(\pm1,\pm1,\pm1)$. There are four possible choices for these directions and when each of those possibilities is assigned to one of the four lattice sites in the cubic unit cell one arrives at the $Pa3$ structure. The pseudopotential between any two protons is

$$u(r)=[b_1/(b_2+r)]^{b_3} \tag{7a}$$

while two protons on the same molecule have the additional term:

$$u(r)=\ln(r)+b_4r-C_pr^2+G\cos^2(\theta)\ . \tag{7b}$$

The various variational parameters have been determined using two different criterion: namely, minimum variational energy and maximum overlap with the exact ground state as generated with DMC. Since this second criterion is less well known it will be briefly described. The overlap between ϕ and Ψ is defined as

$$0=\int\phi\Psi\Big/\left[\int\Psi^2\right]^{1/2}\ . \tag{8}$$

If the logarithm of the trial function (the pseudopotential) is expanded in a linear basis, $\ln(\Psi)=\sum_\beta u_\beta f_\beta(R)$, where u_β are unknown parameters and $f_\beta(R)$ are known functions, then at the maximum of 0 with respect to variations in u_β the following equation holds:

$$\langle f_\beta\rangle_{\rm mix}=\langle f_\beta\rangle_{\rm var}\ . \tag{9}$$

This condition requires[24] that for the radial part of the pseudopotential between pairs i and j to be optimal, the radial distribution functions, as computed by VMC and

TABLE I. Trial function parameters as used in Eqs. 5–7 in units of the Wigner-Seitz radius a in both the atomic and molecular phase. The other parameter, b_3, was always equal to 4.456. The G parameter which controls orientation with the crystal axis was zero for the isotropic fcc phase, but has the tabulated values in the oriented phase.

Density	Atomic		Molecular				
r_s	C_p	C_e	C_p	b_1	b_2	b_4	G
1.13	5.0						
1.31	5.0	0.48	51	6.14	2.25	19.0	−0.33
1.45	5.0	0.55	40	5.55	2.06	10.0	−0.40
1.61	5.5	0.50	42	5.00	1.86	23.5	−0.38
1.77	4.0	0.60	25	4.55	1.69	25.8	
2.00		0.85	13	4.02	1.5	29.1	
2.20		0.75	14	3.66	1.36	32.0	
3.0		1.00	15	2.68	1.00	43.7	

DMC, be equal at all r. Similarly, if the squared displacement of particles from their lattice sites is equal in the VMC and DMC calculation then the C parameters have been correctly chosen. Finally, if the expectation value of $\cos^2(\theta)$ is identical in DMC and VMC, then the orientational parameter G is correctly chosen. Maximum overlap is in some respects an easier criterion to apply than that of minimum variational energy since one knows after doing a VMC and DMC run, which specific parameters need adjusting and in which direction. In the case of orientated molecular hydrogen one can use this criterion to help determine what oriented phase is stable. For example, if the only solution to the equation $\langle \cos^2(\theta)\rangle_{\rm var}=\langle \cos^2(\theta)\rangle_{\rm mix}$ is $G=0$, it seems unlikely that the oriented phase, in fact, exists at that density. The disadvantage of the maximum overlap method is that it requires a well converged DMC run for each iteration of the variational parameters. The best parameters obtained for the various phases of hydrogen are given in Table I. It should be emphasized that converged DMC results are independent of the value of these parameters, it is only the error bars for a given amount of computer time which depends on the trial function.

IV. MOLECULAR PHASE

Using the trial wave function described in Sec. III, VMC, DMC, and GFMC simulations have been performed for four different crystal structures in the molecular phase at densities ranging from 20 cc/mol to 2 cc/mol. The results are summarized in Table II.

A. Crystal structure

The four different crystal structures examined were among those from the high-pressure phases of nitrogen.

(i) fcc isotropic phase. The trial function parameter G

TABLE II. Results of Monte Carlo calculation in the molecular phase. I, O, B, and G refer to the four crystal structures studied [see Sec. IV under (i), (ii), (iii), and (iv), respectively] and the number thereafter to the number of atoms. T is the length of the run (time step times the total number of steps). The energies are in Ry/atom with number in parenthesis being the error in the last digit. The bond length is in bohrs.

r_s	Method	Crystal	T ($\times 10^{-3}$)	$-E_{\rm var}$	$-E^N_{\rm mix}$	P (Mbar)	Bond length
3.0	GFMC	$I64$	8.4	1.125(1)	1.162(1)	0.004	1.42
2.2	DMC	$I64$	2.7	1.114(1)	1.160(1)	0.10	
2.0	DMC	$I64$	6.4	1.117(1)	1.156(1)	0.25	1.40
1.77	DMC	$I64$	3.5	1.080(1)	1.134(1)	0.66	
1.61	GFMC	$I64$	4.3	1.056(1)	1.085(1)		1.26
1.61	DMC	$I216$		1.058(1)			
1.61	DMC	$I64$	1.8	1.058(1)	1.089(1)	1.4	1.24
1.61	DMC	$B54$	1.0	1.071(1)	1.099(3)		1.23
1.61	DMC	$B128$		1.034(1)			
1.61	DMC	$B250$		1.037(1)			
1.45	DMC	$I64$	3.4	1.002(2)	1.032(1)	2.3	1.47
1.45	DMC	$O64$	3.8	1.005(1)	1.035(1)	2.3	1.59
1.45	DMC	$O216$		1.013(1)			
1.45	DMC	$G108$	2.7	0.996(1)	1.028(1)	2.2	1.57
1.31	DMC	$I64$	1.3	0.890(2)	0.939(1)	4.9	
1.31	DMC	$O64$	1.3	0.935(1)	0.960(2)	4.9	1.13
1.31	DMC	$O216$		0.942(1)			
1.31	DMC	$G108$	0.7	0.942(2)	0.962(1)	5.0	1.16
1.31	DMC	$G256$		0.942(1)			

is set to zero which results in the molecule being almost freely rotating about an fcc site. This is the experimentally observed low-pressure phase for hydrogen.

(ii) fcc-oriented phase. The G parameter is nonzero and this means the molecules are oriented relative to a crystal axis in the way described in the preceding section. This is the $Pa3$ (T_h^6) or α-nitrogen structure.

(iii) bccp phase. This is a cubic structure with the molecules aligned along the [111] direction. This arrangement has an energy 0.024 Ry/atom higher than the fcc-oriented structure at $r_s = 1.61$.

(iv) γ-nitrogen phase. This structure is constructed by putting each molecule on a bcc lattice site and orienting the bond directions of the molecules in one of the simple-cubic sublattices in the [110] direction and the other molecules in the [$\bar{1}$10] direction. It has an energy 0.015 Ry/atom higher than the fcc structure at $r_s = 1.45$ and only 0.003 Ry/atom higher at $r_s = 1.31$ but at the latter density the atomic phase has an even lower energy than any of the molecular structures examined.

The results indicate that the oriented $Pa3$ phase is preferred at $r_s = 1.45$, although the energy difference between that and the isotropic phase is small. At higher density the oriented phase has lowest energy. This orientational ordering transition can be placed near 1 Mbar as shown in Fig. 1. It should be noted that the finite time step error, the fixed-node, and the size-dependent effects will tend to cancel in determining the energy difference between these phases so that these limitations should have very little systematic effects. Among the large set of other possible crystal structures only two other phases were examined, the bccp and the γ-nitrogen phase both have definitely higher energies until the atomic phase becomes more stable at $r_s = 1.39$.

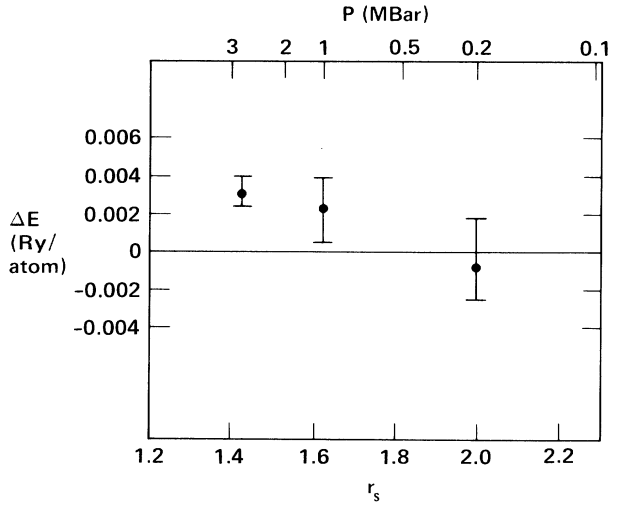

FIG. 1. The difference in energy between the isotropic fcc phase and the oriented $Pa3$ structure as a function of density. The pressure scale is indicated at the top.

B. Approximations

The size effects have been studied only at the variational level because of constraints on computer time but it is expected that these pair-product trial functions will have roughly the same size dependence as would the exact wave functions. At the density of $r_s = 1.61$ there were no observable size effects in the ground-state fcc structure but larger ones in the bccp phase. Both at 2.3 Mbar ($r_s = 1.45$) and at 4.9 Mbars ($r_s = 1.31$) the difference between the 64 and 216 atom systems was 0.008 Ry. The effects in the metallic phase are much greater. In an insulating phase one expects size effects to be smaller because the electrons are localized and at low pressure the molecules interact with each other essentially by weak dipolar forces.

The integration time step used in these calculations varied from 0.01 to 0.02 Ry^{-1}. With these time steps the acceptance rate for moves was greater than 99%. Based on calculations for an isolated hydrogen molecule[11] the finite time-step correction for the ground-state energy will be on the order of 0.001 Ry/atom. To verify this estimate GFMC calculations have been performed at two densities. At the equilibrium density of 20.2 cc/mol ($r_s = 3$), near zero pressure, an energy of -1.162 ± 0.001 Ry/atom was obtained compared with the experimental energy of -1.1645 Ry/atom. At the higher density $r_s = 1.61$ ($v = 3.12$ cc/mol) GFMC gives an energy of -1.085 ± 0.001 Ry/atom compared to DMC of -1.089 ± 0.001 Ry/atom. It is not clear whether this large difference is to be ascribed to time-step error, underestimation of the error bars, statistical fluctuation or the way the fixed-node approximation is treated in GFMC.

The error of the variational wave function ranges from 0.02 to 0.04 Ry and seems to be roughly independent of density. The optimization of the parameters was not carried out uniformly for all runs, so some variation in the quality of the trial function can be expected. The lengths of the computer runs are given in the table in terms of T defined as the time step times the total number of moves. The error of the ground-state energy agrees roughly (within a factor of 2) with the estimate[25] $[2(E_{\mathrm{var}} - E_{\mathrm{mix}})/T]^{1/2}$. Improvements in the wave function will reduce the statistical error.

C. Ground-state energy

The ground-state energies given in Table II for the molecular phases considered and values of r_s between 2.0 and 1.31 were corrected for finite-size effects by adding to them the difference in energy between the 216 and 64 particle variational energy. The results were then fitted by a cubic polynomial in r_s. The fitting coefficients in increasing powers of r_s are equal to 1.1200, -2.9017, 1.2208, and -0.1695. The corrected Monte Carlo points are shown in Fig. 2 and compared with the experimental equation[2] and its empirical extrapolation. The extrapolation is in near agreement with a lattice dynamics calculation[26] with an empirical intermolecular potential derived from shock wave data. The agreement is quite good where experiment is available but in the region $r_s \sim 1.6$

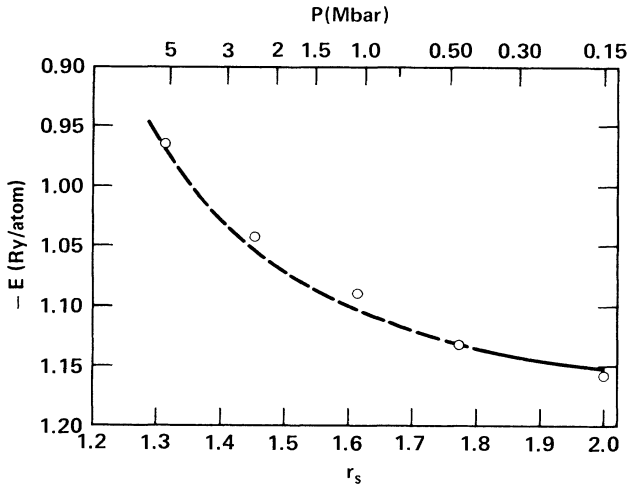

FIG. 2. The energy in the molecule phase (in Ry/atom) vs density (in r_s units). The circles are the Monte Carlo results. The solid line is the diamond-anvil results for pressures less than 400 kbar. The dashed lines are the results (Ref. 6) of lattice dynamics calculation (Ref. 26) with the pair potential fitted to shock-wave data at about 1 Mbar. The pressure scale at the top is based on this pair potential. The dashed line also agrees with an extrapolation of the experimental diamond-anvil measurements (Ref. 6).

(1.2 Mbar) the MC results are 0.010 Ry higher. Tests that have been performed suggest that the MC energies in the molecular phase are accurate to better than 0.005 Ry/atom. Thus, a discrepancy exists at intermediate pressures.

The curve of energy versus density is suggestive of a phase transition at a pressure between 1 and 2 Mbar. Of course there are not nearly enough calculations at different densities to even roughly establish that a transition occurs. The energies involved in the orientational ordering transition are too small to explain the "bump" as can be seen from Fig. 1. Given that the crystal phase is constrained by the trial wave function and the boundary conditions, the only other likely transition would involve a change in the bond length distribution, a contraction of the molecules, possibly coupled with the orientational transition. Some evidence for this is presented in Sec. IV D below. However, since the Monte Carlo run at the density $r_s = 1.61$ is not particularly long, it is possible it has not fully converged to the ground state; the proton degrees of freedom are the slowest to converge and in addition if there is a phase transition there will be a slowing down of the rate of convergence.

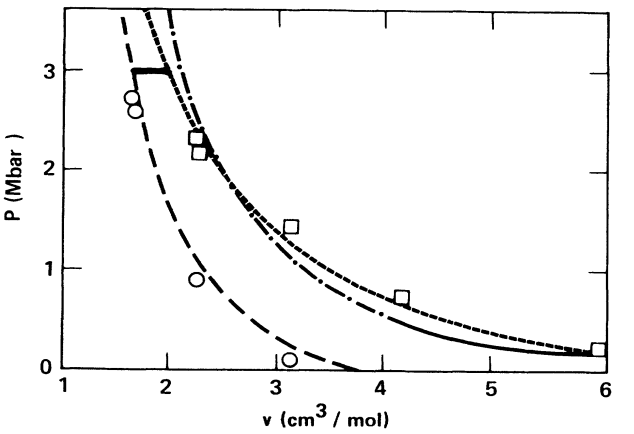

FIG. 3. The pressure vs volume. The open circles are the MC results from the virial theorem in the atomic phase, the lower dashed curve is the derivative of the fit to the atomic energies [Eq. (11)]. Similarly, the open squares and upper dashed curves are for the molecular phase. The solid line shows the transition. The solid curve is the measured (Ref. 2) EOS and its extrapolation (dashed-dotted curve) (Refs. 2 and 26).

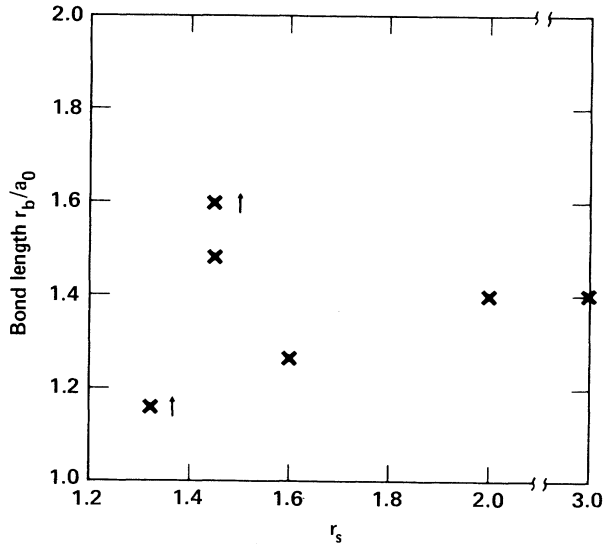

FIG. 4. The bond lengths in bohr radii with the arrows indicating the oriented phase.

The pressure can be computed either by differentiating the energy fit, i.e., $P = 11.71$ Mbar $\mathrm{Ry}^{-1}\, r_s^{-2} dE(r_s)/dr_s$ or by use of the virial theorem. The virial pressure is shown in Table II and a comparison of the two in Fig. 3.

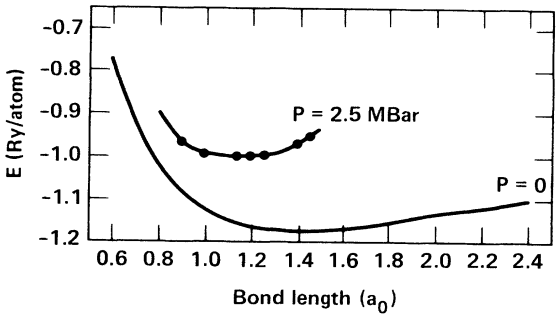

FIG. 5. The Born-Oppenheimer energy as a function of bond length for an H_2 molecule in vacuum ($P = 0$) and at a density of $r_s = 1.45$ ($P = 2.5$ Mbar).

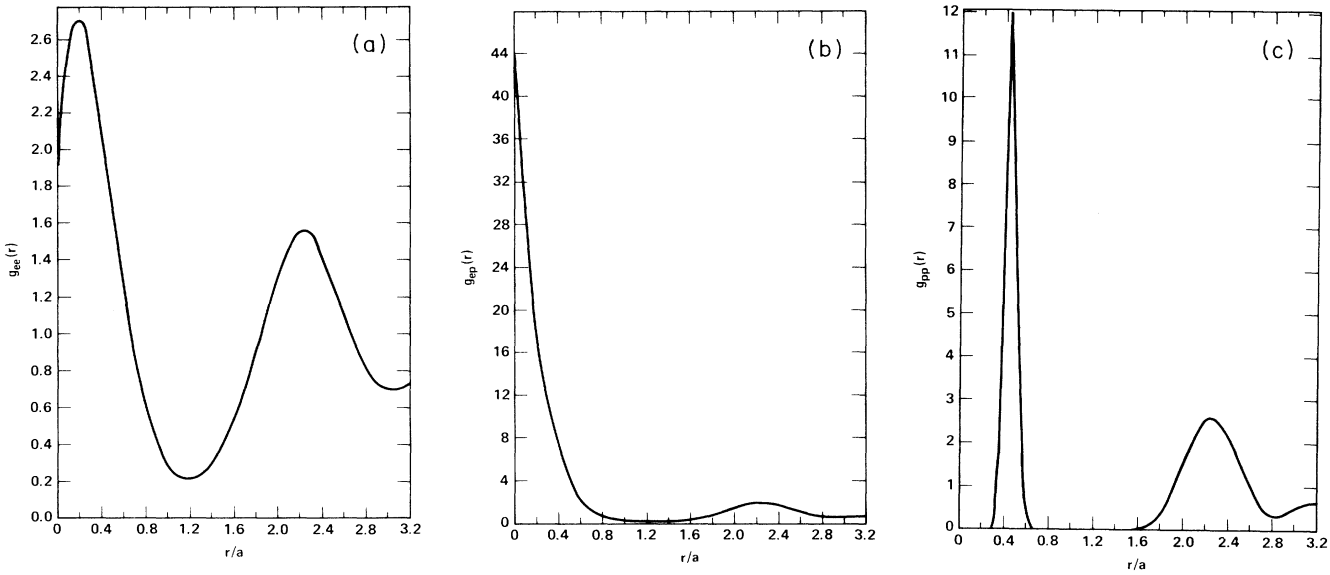

FIG. 6. The pair correlation functions in the molecular ($Pa3$) phase at zero pressure ($r_s = 3.0$). They are sphericalized and normalized to go to unity at large r.

Differentiating the energy is more accurate because it uses the zero variance property of the QMC to reduce fluctuations. The two pressures are in agreement where the polynomial fit to the calculated energies is good.

D. Bond length

The rms value of the molecular bond length is also given in Table II and shown in Fig. 4. Note that these averages are obtained by the extrapolation technique from the variational and mixed averages as explained in the previous section. In general, the bond lengths decrease with increasing density, however, the results at $r_s = 1.45$ do not fit this pattern. The statistical error bars are small for these bond lengths, however, there could well be significant systematic errors, due to either the failure of the extrapolation technique or the slow convergence of the proton degrees of freedom. To avoid the latter problem some runs were carried out at the density $r_s = 1.45$ with the Born-Oppenheimer approximation, that is by fixing the protons in the oriented $Pa3$ structure with a given bond length and setting their mass to infinity. The energy as a function of bond length is shown in Fig. 5. As a comparison, the Born-Oppenheimer energy of an isolated molecule is shown. It is seen that the effect of pressure on the molecule is to shrink the bond, but the restoring force also diminishes, leading to a much more anharmonic bonding force. These Born-Oppenheimer simulations are naturally much less expensive since they converge to the ground state within a few inverse Rydbergs, corresponding to about 50 time steps, rather than thousands of iterations, if the protons are moving with their correct mass. The unusual dependence of bond length on density could be related to the excess energy at intermediate density discussed above in Sec. IV C.

E. The pair correlation function

Shown in Fig. 6 are the three types of pair correlation functions (that is e-e, e-p, and p-p) for molecular hydrogen at zero pressure. The Fourier transform of these functions, the structure function will be discussed later in relation to the dielectric susceptibility. The peak at small r represents correlations between particles within the same molecule while that for distances between $2.0a$ and $2.6a$ represents correlations between nearest-neighbor molecules.

V. THE ATOMIC PHASE

In the atomic phase the RPA pseudopotentials[22] were used between all pairs of particles. Gaussians were used for the protonic orbitals while plane waves, filled up to the Fermi level, were used for the electronic orbitals. Table III contains the variational energies and the DMC results.

A. Finite-size scaling

In the metallic phase the extrapolation to the thermodynamic limit is much larger than in the molecular phase and must be done carefully if the results are to be accurate. Size effects are bigger in this phase simply because the electrons are delocalized and thus sensitive to boundary effects.

The extrapolation method is based on the picture provided by Fermi-liquid theory. According to Landau,[27] the energy of a system can be written as an energy functional of occupation numbers of quasiparticles, which behave just like an ideal Fermi gas. For small excitations from the ground state the functional can be linearized and is characterized by a few Fermi-liquid parameters. Consider how the energy of such an ideal Fermi-liquid

TABLE III. Monte Carlo results in the atomic phase. N is the number of atoms, T is the total length of the run [(time step)$\times$ (ensemble size)$\times$(number of steps)]. $E^N_{\rm mix}$ is the fixed-node energy for the finite system, $E^\infty_{\rm mix}$ is extrapolated to the bulk limit using Eq. (10). P is the virial pressure. Lindemann's ratio is the rms value of the proton displacement from the lattice site divided by the nearest-neighbor distance.

r_s	Crystal	N	T ($\times 10^{-3}$)	$-E_{\rm var}$	$-E^N_{\rm mix}$	$-E^\infty_{\rm mix}$	P (Mbar)	Lindemann's ratio
				Static lattice of protons				
1.0	fcc	108	1.0	0.635(2)	0.670(1)	0.727	19.5	
1.13	fcc	108	1.6	0.816(1)	0.849(1)	0.893	8.4	
1.13	bcc	54	1.2	0.949(2)	0.983(3)	0.891	8.5	
1.13	bcc	128	1.6	0.835(2)	0.876(3)	0.897	8.3	
1.30	fcc	108	2.0	0.935(1)	0.970(2)	1.002	2.7	
1.31	bcc	128	1.2	0.957(1)	0.988(1)	1.002	2.6	
1.31	fcc	256	0.8	0.957(1)	0.992(1)	1.002	2.6	
1.45	bcc	54	3.4	1.065(1)	1.094(1)	1.035	0.88	
1.45	fcc	108	1.5	0.982(1)	1.011(1)	1.039	0.85	
1.61	fcc	108	2.8	0.999(1)	1.033(1)	1.052	0.07	
1.77	fcc	108	3.2	0.998(1)	1.033(1)	1.048	−0.18	
2.00	fcc	108	4.0	0.980(1)	1.021(1)	1.033	−0.29	
				Dynamic lattice of protons				
1.13	bcc	54	0.6	0.782(1)	0.813(1)	0.856	9.13	0.15
1.31	sc	64	5.0	0.967(1)	0.985(1)	0.962	2.84	0.16
1.31	fcc	108	0.8	0.913(1)	0.942(1)	0.973	3.05	0.13
1.45	bcc	54	2.3	1.050(1)	1.071(1)	1.012	1.17	0.16
1.45	fcc	108	1.2	0.960(1)	0.990(1)	1.016	1.18	0.15
1.61	bcc	54	1.2	1.057(1)	1.081(1)	1.032	0.25	0.15
1.77	fcc	108	0.8	0.985(1)	1.019(1)	1.035	−0.03	0.16

changes when one goes from a finite system in periodic boundary conditions to an infinite system. For a finite system the allowed values of momentum lie on a lattice reciprocal to that of the simulation cell and the ground state is obtained by filling successive "shells" of these lattice points. (A shell consists of all lattice points related to each other by symmetry.) As long as the shells are filled in a symmetric fashion then the only Fermi-liquid parameter that comes in should be the effective mass. This implies that the size corrections of the interacting system should be simply proportional to the size correction of the noninteracting system, at least for large enough systems. The difference in energy per particle between an infinite and a finite ideal Fermi gas of N particles in periodic boundary conditions is of order $1/N$ with a coefficient[19] which varies between ± 1 as N changes.

For charged systems, in addition to this number dependent effect on the kinetic energy, there is also an effect in the potential energy,[19] since the potential is long ranged. In simulations with periodic boundary conditions, the coulomb interaction is replaced by the Ewald image potential for finite systems. To have charge neutrality a particle must interact with its own image. Thus, in calculating the potential energy one term out of N is appropriate to a perfect lattice, not to a Fermi liquid, as it should be. This intuitive result is supported by both Hartree-Fock calculations, valid at small r_s, and harmonic lattice calculations, valid at large r_s, which show that the size dependence of the potential energy of the homogeneous electron gas is proportional to $1/N$.

Adding together these kinetic and potential-energy size corrections, implies that the energy per particle for a finite system is related to the bulk energy per particle by

$$E_N = E^\infty + c_1(r_s)(T_N - T_\infty)/r_s^2 + c_2(r_s)/(Nr_s)\ , \quad (10)$$

where c_1 and c_2 are functions of the density to be determined from the simulations and T_N is the kinetic energy of the ideal gas, at $r_s = 1$. We have multiplied c_1 and c_2 by r_s^2 and r_s, respectively, so that c_1 and c_2 will be roughly independent of r_s in the high-density limit.

VMC calculations have been performed with many different values of N to test the accuracy of Eq. (10) and to determine the unknown parameters E^∞, c_1, and c_2. VMC was used rather than DMC since it is much less time consuming, particularly for large systems. Because the pair product trial function has the correct long-wavelength properties it should give the same size dependence as an exact calculation. One can observe by examining Table III that the size dependence is the same for the VMC and DMC calculation to within the statistical error of 0.002 Ry/atom even though the variational energy changes by 0.101 Ry/atom in going from 54 to 108 atoms. The size-dependence correction is itself very large. Table IV contains the results of variational calculations for N ranging from 32 to 432, for $r_s = 1.31$ and Fig. 7(a) illustrates the correlation between the variational kinetic energy versus that kinetic energy of an ideal Fermi gas with the same number of particles. Figure 7(b) shows the strong correlation between the variational potential energy and $1/N$. In fact, Eq. (10) fits the total variational energies better than the variational and potential energy separately. For $r_s = 1.31$ the fitted values of c_1 and c_2 are 1.118 and -1.146. The corrected infinite system energies are also displayed in Table IV. It is seen that the maximum variation not including that of the sc phase is only 0.0033 Ry. Thus the uncertainty due to the finite system

TABLE IV. Results of variational calculations in the atomic phase at $r_s = 1.31$ for seven different sizes of systems. Columns labeled with ∞ show the extrapolation to the bulk limit. T_N is the ideal-gas kinetic energy.

Crystal	N	$-E^N_{\rm var}$	$-V^N_{\rm var}$	T_N/r_s^2	$-E^\infty_{\rm var}$	$-V^\infty_{\rm var}$	$-P^\infty_{\rm var}$
fcc	32	0.9442(3)	2.446(1)	1.318	0.9501	2.430	2.76
bcc	54	1.0209(3)	2.451(1)	1.239	0.9506	2.430	2.75
sc	64	0.9664(7)	2.437(4)	1.280	0.9435		
fcc	108	0.9199(4)	2.431(2)	1.323	0.9511	2.431	2.75
bcc	128	0.9368(5)	2.432(2)	1.307	0.9516	2.430	2.74
bcc	250	0.9390(5)	2.430(2)	1.299	0.9483	2.429	2.77
fcc	256	0.9406(9)	2.430(3)	1.300	0.9513	2.429	2.74
bcc	432	0.9477(11)	2.429(4)	1.292	0.9509	2.428	2.74

size has been reduced by a factor of 30!

The reason the total energies are fit better by Eq. (10) than are the variational and kinetic energies separately is that some of the potential-energy correction gets mixed into the kinetic energy and vice versa. For a system of charges, the kinetic energy is related to the total energy by

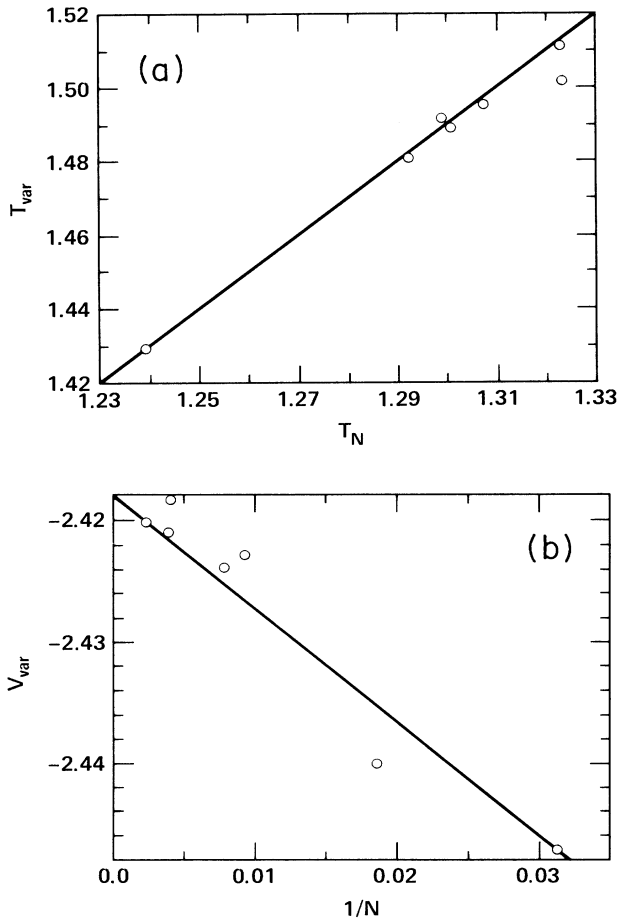

FIG. 7. (a) The variational kinetic energy of metallic hydrogen as computed with a pair product trial function vs the kinetic energy of an ideal Fermi gas with the same number of electrons at the density of $r_s = 1.31$. The line has a slope of unity. (b) The variational potential energy vs $1/N$, where N is the number of hydrogen atoms at the density of $r_s = 1.31$.

$T = -d(r_s E)/dr_s$. Thus the size dependence of the kinetic energy also follows Eq. (10) with $c_1^T = c_1 - r_s c_1$ and $c_2^T = r_s c_2$. Since the size dependence of the potential and kinetic energies are needed to find the pressure with the virial theorem, it is necessary to fit separately the kinetic and potential energies to Eq. (10), giving new coefficients c^T and c^V. The potential-energy corrections at $r_s = 1.31$ are $c^V = (0.165, -0.890)$. Variational calculations have also been carried out at a higher density $r_s = 1.13$, obtaining for the fitting coefficients $c = (1.104, -1.153)$ and $c^V = (0.050, -0.80)$ showing the assumed r_s dependence of c_1 and c_2 is approximately correct. This method provides a simple way of calculating the Fermi liquid parameters since c_1 should be equal to the effective mass, which is near unity in metallic hydrogen.

B. Lattice type

All calculations have used either fcc, bcc, or sc lattices. The simple cubic lattice has higher energy at $r_s = 1.31$ (by about 0.010 Ry/atom) but the size effects and the error bars are too large to determine whether fcc or bcc is more stable. Adding a term dependent on the lattice type to Eq. (10) does not appreciably improve the fit to the energies. Thus the energies of the two lattices are the same to the accuracy of about 0.002 Ry/atom at the density $r_s = 1.31$. For comparison, by perturbation theory[28] the static fcc lattice was found to be more stable in the range $1 < r_s < 1.6$ by 0.0012 Ry. Perturbation calculations which ignore proton zero-point motion, have found unusual planar structures that are more stable than either fcc or bcc, however, isotropic structures are favored once the protons are allowed to move. A density-functional calculation[29] found the simple cubic structure most stable at $r_s = 1.31$ by 0.003 Ry/atom. Thus, this theory cannot reliably determine even crystal structures for hydrogen.

C. Ground-state energy

Table III contains the ground-state energies corrected for finite system size, assuming $c_1 = 1.10$ and $c_2 = -1.15$ are independent of r_s. The energies for densities in the range $1.0 < r_s < 2.0$ are fit to the expression:

$$E(r_s) = 2.21 r_s^{-2} - 2.70722 r_s^{-1} + d_1 + d_2 r_s + d_3 r_s^2 , \qquad (11)$$

where the first two terms give the exact behavior[30] for a static lattice in the high-density limit. The values of

$d_1 = -0.2166$, $d_2 = 0.0566$, and $d_3 = -0.0301$ were obtained for the dynamic hydrogen lattice.

The fitted energies are shown in Fig. 8 and compared to other theoretical predictions. The results in closest agreement with the MC energies are those of perturbation theory[28] which are quite accurate in the range $1.4 < r_s < 1.6$ and are high by about 0.015 Ry at $r_s = 1.1$. Variational correlated basis calculations[31] are too *low* by 0.02 Ry. Approximations have significantly compromised the variational principle since the variational energy with this type of trial function should be 0.03 Ry above the exact energy. Local-density-functional results lie even further below the exact energies, by 0.03 Ry/atom and the error is density dependent, getting much worse as r_s gets larger than 1, and even give the wrong crystal structure. The atomic equation of state (EOS) is shown in Fig. 3.

D. Effect of proton motion

The difference in energy between calculations on a static lattice and for the real lattice defines the proton zero-point energy and is shown in Fig. 9. The results are larger than the estimate of this energy difference using either the Debye model[32] or the self-consistent harmonic approximation.[30] Also given in Table III is the Lindemann's ratio, that is the rms displacement from the lattice divided by the nearest-neighbor distance. For hydrogen this value is about 0.15, considerably less than that of helium at melting, where the ratio is 0.26.

E. Effect of finite time step and fixed-node approximation

Simulations with different but small time steps were used to correct the energy for the timestep error. A GFMC test run at one density showed no observable effect of timestep errors or fixed-node errors. This conforms to a similar nodal-release calculation for the electron gas,[12] where the energy as lowered by about 0.001 Ry/atom. The error in the fixed-node approximation should be less important in hydrogen than in the electron gas since the protons partially localize the electrons. The final accuracy in the ground-state energy is estimated to be 0.003 Ry/atom, at least twice as small as the error in the molecular phase. The calculations are more accurate in the atomic phase because the motion of the protons is much more restricted.

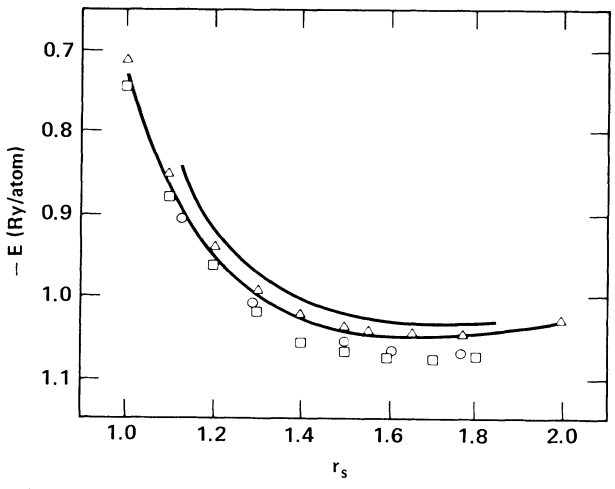

FIG. 8. The energy of metallic hydrogen in the atomic phase as a function of density. The upper line is a fit to the MC results for the finite mass proton lattice of hydrogen while the lower line is for a static lattice (protons of infinite mass) either fcc or bcc. Open triangles represent results of perturbation theory (Ref. 28); open circles the variational correlated theory (Ref. 31); open squares the density-functional theory (Ref. 29).

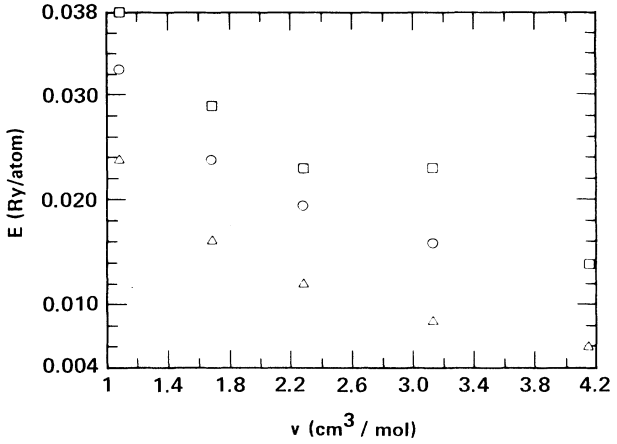

FIG. 9. The zero-point vibrational energy of atomic hydrogen (Ry/atom) as a function of density. The open squares are the MC results, the open circles the results of a Debye model (Ref. 32), and the open triangles of a lattice dynamics calculation (Ref. 30).

The amount of energy missed by the RPA pseudopotential is about 0.035 Ry/atom, 35% of the total electron-correlation energy. Thus the electronic part of the trial wave function is equally accurate in the atomic and molecular phase. However for the electron gas the RPA pseudopotential picks up 95% of the correlation energy at this density.[16] This much larger variational energy for hydrogen probably comes from electron-proton correlations. The simple pair-product trial function used here has an inadequate treatment of the band structure which raises the variational energy by about 0.03 Ry/atom.

F. Atomic-molecular transition

Using the fits to the molecular and atomic energies, it can be determined that hydrogen changes from an fcc molecular phase to a cubic atomic crystal at a pressure of 3.0 Mbar. The atomic phase is stable for $r_s < 1.30$ (1.65 cc/mol) and the assumed molecular phase is stable for $r_s > 1.39$ (2.01 cc/mole). Thus, the relative volume change is 20%. There have been many previous estimates of this transition density some of which are similar to the present one. It is difficult to give good error bounds to this estimate of the transition density. The errors coming solely from statistical fluctuations of the Monte Carlo runs are quite small (on the order of 0.002 Ry/atom) but

TABLE V. The energy needed to add or subtract a zero-momentum electron for $N/2$ molecules of H_2 and the resulting energy gap at $k=0$. The protons were held rigid in the $Pa3$ structure with the given bond length (r_{HH}).

r_s	N	r_{HH} (Å)	$E^- - E$ (eV)	$E^+ - E$ (eV)	E_{gap} (eV)
3.0	8	1.4	−3.0	12.6	9.6±2.0
3.0	64	1.4	1.2	13.6	14.8±1.0
1.45	64	1.3	−1.0	1.9	0.9±1.0

systematic effects can be quite a bit larger, the largest ones are (i) poor convergence of the proton degrees of freedom in the molecular phase, (ii) uncertainty about the crystal structure of the molecular phase, (iii) finite-size effects, (iv) incomplete treatment of antisymmetry (Fermi statistics), and (v) inadequate fit to the calculated energies. Attributing an uncertainty of no more than 0.004 Ry/atom to each phase, and assuming that this error is roughly independent of density in the 3-Mbar region, these factors could change the transition pressure by 15%, the molecular critical volume by 8%, and the atomic critical volume by 5%.

G. Pair correlation function

The pair correlation function in the atomic sc phase is shown in Fig. 10 at the lowest stable atomic density, $r_s=1.31$. The electron-electron function is similar to that of an electron gas at the same density.

VI. DIELECTRIC RESPONSE OF HYDROGEN

It has been suggested that molecular hydrogen could become a metal at high pressures before undergoing a transition to an atomic phase since as the density increases, its bands broaden, closing an indirect gap and the system would undergo a transition to a metallic state.[7] Such a phenomenon has been observed in iodine at high pressures.

For a system of rigid molecules in the $Pa3$ structure, the energy change in adding and in removing an electron was calculated with DMC as shown in Table V. Both the electron and hole were assumed for simplicity to be in a zero-momentum state, thus the sum of the energy changes is the band gap at $k=0$. For a system of 64 molecules at zero pressure ($r_s=3$) the band gap was found to be 15±1 eV while at 2.4 Mbar ($r_s=1.45$) the band gap was 1±1 eV. It is difficult both to assess the reliability of this calculation and to compare with experiment. The restriction to zero-momentum particle and hole states increases the gap at $r_s=3$ by 1.5 eV in a band-structure calculation[7] and 3.5 eV in a Hartree-Fock calculation,[33] the band gaps in these two methods are also very different. Band structure predicts a minimum gap of 9.2 eV while Hartree-Fock predicts a gap of 15 eV, possibly because neither of these methods can calculate reliable electron affinities of molecules. It is also difficult to determine the band gap from either the energy-loss experiments,[34] which show an edge at 10.9 eV plus other features at 15 eV or from absorption in the optical spectrum[35] which has features at 10, 12, 15, and 17 eV. At the higher pressure of 2.4

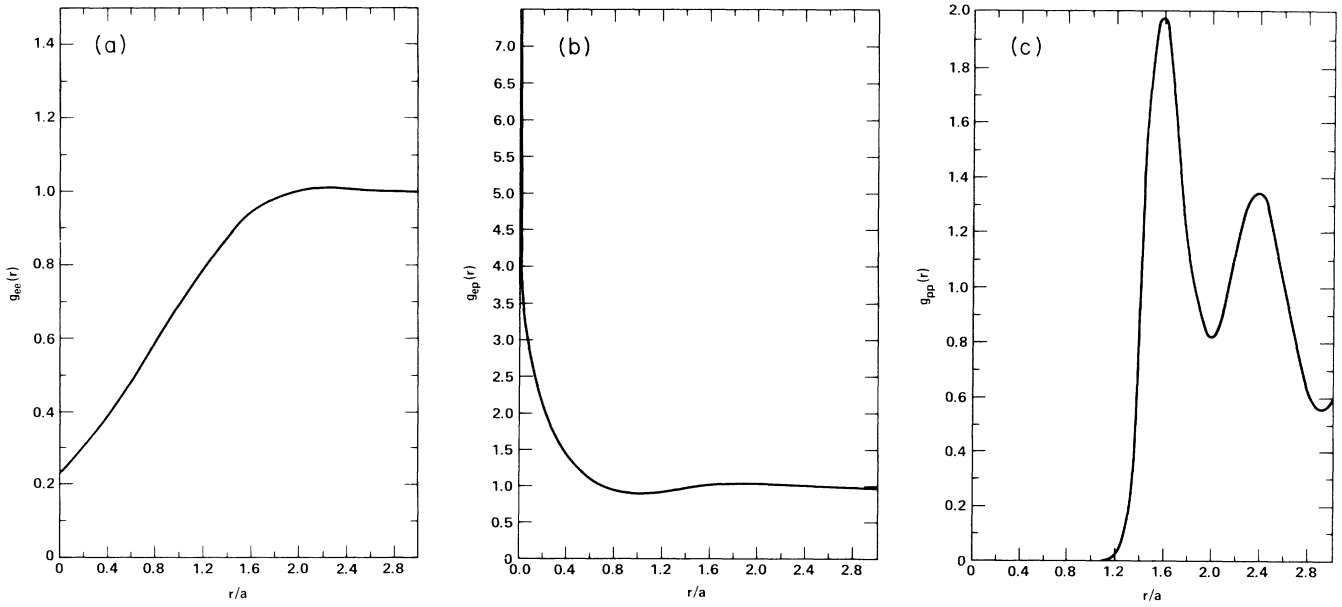

FIG. 10. The pair correlation function in the atomic sc phase at the density $r_s=1.31$. Each of the three functions is sphericalized and normalized to be unity at large r.

Mbar the gap at $k=0$ is almost closed in our calculation. In density-functional theory[7] the gap is predicted to be about 6 eV, but an indirect gap has almost closed.

Not withstanding the approximations employed in this gap calculation (small systems, rigid molecules, zero-momentum excitations, and the fixed-node approximation) the results indicate that this direct subtraction method could be useful. The most worrisome problem is the restriction to small systems as can be seen from Table V. The short run of 8 atoms shows that one must clearly go to larger systems. It would be highly desirable to explore the finite-size effects by doing the calculations on larger systems because such effects are much larger for charged systems. The present method however cannot be practically used for very large systems since the statistical error for a given amount of computer time, t, can be shown to be proportional to $(N^4/t)^{1/2}$; thus computer time requirements become excessive. A direct calculation of the energy necessary to promote an electron into the conduction band would solve both the problem of charge neutrality and the restriction to small system size and appears feasible. In addition, information about the entire band structure could be obtained by varying the momentum of the hole and electron.

Alternatively, the behavior of the dielectric constant can be used to indicate the onset of metallic conductivity. An inequality between the structure factor, which can easily be found with Monte Carlo calculations, and the static dielectric function restricts the range when the fcc molecular system is predicted to conduct at zero temperature.

The dielectric function, $\epsilon(k,\omega)$, for any system with translational invariance (valid here since the protons are free to move) can be related[36] to the dynamical structure factor, $S(k,\omega)$, by

$$1-\frac{1}{\epsilon(k,\omega)}=\lim_{\delta\to 0}\left\{[4\pi/(k^2v)]\times\int_{-\infty}^{\infty}d\omega' S(k,\omega')[(\omega'+\omega+i\delta)^{-1}+(\omega'-\omega-i\delta)^{-1}]\right\} . \tag{12}$$

The static dielectric function (i.e., when $\omega=0$) is then proportional to the ω^{-1} moment of $S(k,\omega)$; the singularity at $\omega'=0$ is treated as given by the limit in Eq. (12). The dynamic structure factor can be expanded in terms of the full set of eigenvalues and eigenfunctions:

$$S(k,\omega)=\sum_n \delta(\omega-E_n+E_0)\,|\langle n\,|\,\rho_k\,|\,0\rangle\,|^2 , \tag{13}$$

where $\rho_k=\sum_i e_i \exp(i\mathbf{k}\cdot\mathbf{r}_i)/\sqrt{N}$ is the fourier transform of the charge density, N is the number of atoms, and e_i is the charge of the ith particle. The first two moments of $S(k,\omega)$ satisfy the two sum rules

$$S(k)=\int_{-\infty}^{\infty}d\omega\, S(k,\omega)=\langle\rho_k\rho_{-k}\rangle ,$$
$$S_1(k)=\int_{-\infty}^{\infty}d\omega\,\omega S(k,\omega)=\sum_i \hbar^2k^2e_i^2/2m_iN . \tag{14}$$

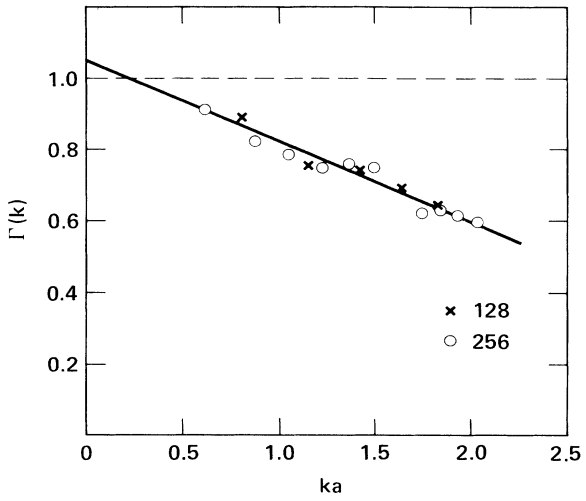

FIG. 11. The low wave-number (ka) behavior of the charged structure factor $\Gamma(k)$ [defined in Eq. (16)] for the atomic metal at $r_s=1.31$ for two different sized systems.

Since from Eq. (13), $S(k,\omega)$ is non-negative, the following inequality holds for any value of b:

$$\int_0^{\infty}d\omega\, S(k,\omega)(\omega^{-1/2}-b\omega^{1/2})^2\geq 0 . \tag{15}$$

Choosing the value of b which minimizes the integral, that is, $b=S(k)/S_1(k)$, and using Eqs. (12) and (13) and the observation that $S(k,\omega)$ is zero for $\omega<0$ leads to the following inequality for any translationally invariant system of charges at zero temperature:

$$1-\frac{1}{\epsilon(k,0)}\geq 8\pi[S(k)]^2/[k^2vS_1(k)]\equiv\Gamma(k)^2 . \tag{16}$$

The static structure factor thus provides a rigorous lower

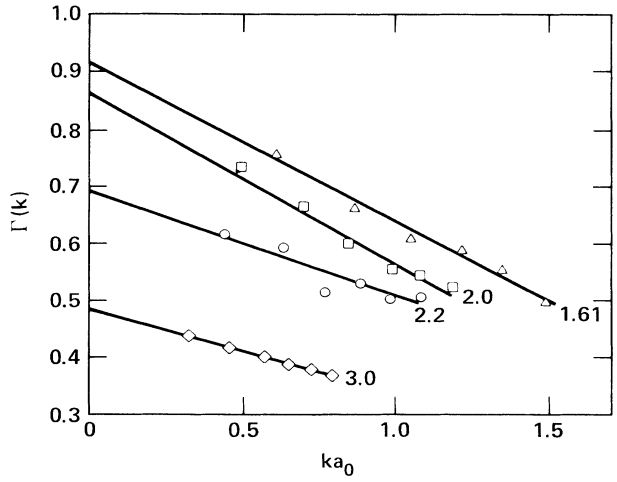

FIG. 12. The low wave-number (ka) behavior of the charged structure factor $\Gamma(k)$ [defined in Eq. (16)] for molecular H_2 for four values of density ($r_s=3.0$, 2.2, 2.0, and 1.61). The lines are fitted to the points.

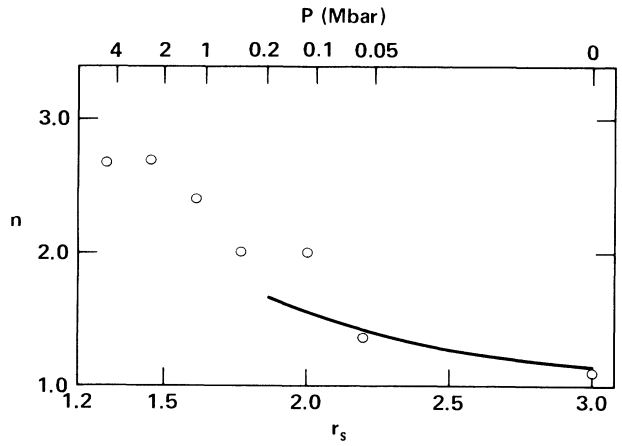

FIG. 13. The index of refraction, n, vs density for hydrogen in the molecular phase. The solid line represents experiment (Ref. 34). The open circles are the MC lower bond obtained from Eq. (16) by extrapolating as in Fig. 10. The pressure scale is the same as used in Fig. 2.

bound to the dielectric function. If at particular wavelength $S(k,\omega)$ is sharply peaked at a single frequency then it is easy to show from Eq. (15) that the inequality becomes an equality. Such is the case in a metal where plasmons are the only long-wavelength excitations. An illustration of that is given in Fig. 11 for $\Gamma(k)$ in the atomic phase at a density of $r_s=1.31$. Linear extrapolation of $\Gamma(k)$ to zero wave number gives 1.05, which is consistent within the errors and the extrapolation to a value of Γ of 1, that is an infinite dielectric constant or, in other words, a metallic state.

Shown in Fig. 12 is $\Gamma(k)$ in the molecular phase for four densities, $r_s=3.0$, 2.2, 2.0, and 1.61. Most of the simulations have been performed with 64 atoms, which corresponds to a minimum value of k of 0.97, and hence a relatively far extrapolation to $k=0$. At zero pressure ($r_s=3$) the extrapolated $\Gamma(0)$ values of 0.47 yields a lower bound to the index of refraction of 1.14. This value is to be compared with the experimental value of 1.12. In Fig. 13 a comparison of the computed lower bound to the index of refraction with experiment[37] is shown. Higher calculated index of refraction values than experiment around 100 kbar could be accounted for either by statistical fluctuations or more likely by extrapolation errors. Also it has been assumed that the structure factor is isotropic at small k. The index of refraction levels out above 500 kbar at about 2.7. A sharp transition to a metallic state is not expected to be obtained since a finite system contains so few points in reciprocal-lattice space near the Fermi surface. However, this method based on the charged structure factor gives a rough indication of the onset of the metallic state.

VII. CONCLUSION

This work represents an attempt to calculate the properties of a real material from first principles with quantum Monte Carlo. Much more work needs to be done to improve the trial functions, to improve the methods for dealing with fermions, to improve the problem faced by the separation of proton and electron time scales and to simulate much larger systems. However, the feasibility of a realistic calculation of the atomic and molecular phases and the transition between them in hydrogen without using experimental information has been demonstrated. Similar calculations can be done for other low Z elements and are now in progress for lithium. It is straightforward to simulate also mixtures of hydrogen, helium and lithium. It has been shown[25] that this method scales as $Z^{5.5}$, thus making it impractical for large Z elements unless elimination of the inner electrons by the use of pseudopotentials is employed. Finite-temperature extensions of these techniques are well developed for boson systems and could be extended as well to charged fermion systems.

ACKNOWLEDGMENTS

This work was performed under the auspices of the U.S. Department of Energy by the Lawrence Livermore National Laboratory under Contract No. W-7405-Eng-48. We wish to thank G. Sugiyama for performing the energy-gap calculations.

[1]E. Wigner and H. B. Huntington, J. Chem. Phys. **3**, 764 (1935).
[2]J. van Straaten, R. J. Wijngaarden, and I. F. Silvera, Phys. Rev. Lett **48**, 97 (1982).
[3]S. K. Sharma, H. K. Mao, and P. M. Bell, Phys. Rev. Lett. **44**, 886 (1980).
[4]W. J. Nellis *et al.*, Phys. Rev. A **27**, 608 (1983); J. Chem. Phys. **79**, 1480 (1983).
[5]I. F. Silvera, Rev. Mod. Phys. **52**, 393 (1980).
[6]I. F. Silvera and R. J. Wijngaarden, Phys. Rev. Lett. **47**, 39 (1981).
[7]C. Friedli and N. W. Ashcroft, Phys. Rev. B **16**, 662 (1977).
[8]N. W. Ashcroft, Phys. Rev. Lett. **21**, 1748 (1968).
[9]E. G. Brovman, Y. Kagan, A. Kholas, Zh. Eksp. Teor. Fiz. **61**, 2429 (1971) [Sov. Phys—JETP **34**, 1300 (1972)].
[10]M. H. Kalos, M. A. Lee, and P. A. Whitlock, Phys. Rev. B **24**, 115 (1981).
[11]P. J. Reynolds, D. M. Ceperley, B. J. Alder, and W. A. Lester, J. Chem. Phys. **77**, 5593 (1982).
[12]D. M. Ceperley and B. J. Alder, Phys. Rev. Lett. **45**, 566 (1980).
[13]N. Metropolis, A. W. Rosenbluth, M. N. Rosenbluth, A. H. Teller, and E. Teller, J. Chem. Phys. **21**, 1087 (1953).
[14]W. L. McMillan, Phys. Rev. **138**, A442 (1965).
[15]D. M. Ceperley, G. V. Chester, and M. H. Kalos, Phys. Rev. B **16**, 3081 (1977).
[16]D. M. Ceperley, in *Recent Progress in Many-Body Theories*, Vol. 142 of *Lecture Notes in Physics*, edited by J. G. Zabolitzky (Springer-Verlag, Berlin, 1981), p. 262.
[17]D. M. Ceperley and M. H. Kalos, in *Monte Carlo Methods in Statistical Physics*, edited by K. Binder (Springer-Verlag, Berlin, 1979).
[18]D. M. Ceperley and B. J. Alder, J. Chem. Phys. **81**, 5833

(1984).
[19]D. M. Ceperley, Phys. Rev. B **18**, 3126 (1978).
[20]M. Parrinello and A. Rahman, Phys. Rev. Lett **45**, 1196 (1980).
[21]F. J. Pinski and C. E. Campbell, Phys. Lett. **79B**, 23 (1978); L. J. Lantto, Phys. Rev. B **22**, 1380 (1980).
[22]D. M. Ceperley, Physica **108B**, 875 (1981).
[23]J. des Cloizeaux, Phys. Rev. **135A**, 698 (1964).
[24]L. Reatto, Phys. Rev. B **26**, 130 (1982).
[25]D. M. Ceperley, J. Stat. Phys. **43**, 815 (1986).
[26]M. Ross, F. H. Ree and D. A. Young, J. Chem. Phys. **74**, 1487 (1983).
[27]L. D. Landau and E. M. Lifshitz, *Statistical Physics,* 2nd ed. (Addison-Wesley, Reading, Mass, 1970), p. 194.
[28]J. Hammerberg and N. W. Ashcroft, Phys. Rev. B **9**, 409 (1974).
[29]B. I. Min, H. J. F. Jansen, and A. J. Freeman, Phys. Rev. B **30**, 5076 (1984).
[30]L. G. Caron, Phys. Rev. B **9**, 5025 (1974).
[31]V. T. Rajan, C.-W. Woo, Phys. Rev. B **18**, 4048 (1978).
[32]G. A Neece, F. J. Rogers, and W. G. Hoover, J. Comp. Phys. **7**, 621 (1971).
[33]P. Giannozzi and S. Baroni, Phys. Rev. B **30**, 7187 (1984).
[34]L. Schmidt, Phys. Lett. **36A**, 87 (1971).
[35]G. Baldini, Jpn. J. Appl. Phys. Suppl. **14**, 613 (1965).
[36]G. D. Mahon, *Many-Particle Physics* (Plenum, New York, 1981).
[37]H. Shimizu, E. M. Brody, H. K. Mao, and D. M. Bell, Phys. Rev. Lett. **47**, 128 (1981).